Octahedral bis(2-thenoyltrifluoroacetonato)-ethylenediamine Co(II), Ni(II) and Cu(II) complexes: Synthetic, structural, electrochemical, and theoretical studies

G. Ahumada, Thierry Roisnel, S. Kahlal, D. Carrillo, R. Córdova, J.-Y. Saillard, J.-R. Hamon, C. Manzur

Manuscript Ref: ICA_2017_175

Revised version

Octahedral bis(2-thenoyltrifluoroacetonato)-ethylenediamine Co(II), Ni(II) and Cu(II) complexes: synthetic, structural, electrochemical, and theoretical studies[#]

Guillermo Ahumada[a,b], Thierry Roisnel[b], Samia Kahlal[b], David Carrillo[a], Ricardo Córdova[a], Jean-Yves Saillard[b],* Jean-René Hamon[b],* Carolina Manzur[a]*

[a]Laboratorio de Química Inorgánica, Instituto de Química, Pontificia Universidad Católica de Valparaíso, Campus Curauma, Avenida Universidad 330, Valparaíso, Chile

[b]Institut des Sciences Chimiques de Rennes, UMR 6226 CNRS-Université de Rennes 1, Campus de Beaulieu, 35042 Rennes Cedex, France

[#]Dedicated to our distinguished colleague Prof. Carlo Meali on the occasion of his 70th birthday

Corresponding authors

Phone: +56 32 227 49 32, e-mail address: cecilia.manzur@pucv.cl (C. Manzur)

Phone: +33 22 323 59 58, e-mail address: jean-rene.hamon@univ-rennes1.fr (J.-R. Hamon)

Phone: +33 22 323 67 28, e-mail address: saillard@univ-rennes1.fr (J.-Y. Saillard)

1

Abstract

We report the synthesis of three new octahedral bis(2-thenoyltrifluoroacetonato)-ethylenediamine metal(II) complexes [M(TTA)$_2$(en)] (M = Co, **2a**; Ni, **2b**; Cu,**2c**) resulting from the coordination of the diamine onto the bis(β-diketonate) precursors [Co(TTA)$_2$(CH$_3$OH)$_2$] (**1a**), [Ni(TTA)$_2$(H$_2$O)$_2$] (**1b**) and [Cu(TTA)$_2$] (**1c**), respectively. The six-coordinate paramagnetic complexes **2a-c** have been isolated as neutral, air and thermally stable solids in high yields (> 80%) and have been fully characterized by elemental analysis, ESI$^+$ HRMS, FT-IR and UV-vis spectroscopy. Single-crystal X-ray diffraction studies indicate that the metal(II) ion sits in a pseudo-octahedral environment; the copper derivative **2c** showing a significant elongation along the O-Cu-O axis due to Jahn-Teller distorsion associated with the "eg" electron occupation of the d$_{z2}$-type MO. The three complexes 2a-c display similar cyclic voltammetric behavior exhibiting two irreversible anodic waves, tentatively assigned to the M(II)/M(III) redox couples and to the oxidation of soluble short oligomeric species generated during the first redox process, respectively. No deposits of polymeric species on the electrode surface occured. The electronic structures of **2a-c** and their cations have been analysed through DFT calculations, allowing providing a consistent view of their structure and properties. TDDFT calculations have been used to interpret the major features of their UV-vis spectra.

1. Introduction

β-diketones are important compounds in organic synthesis where they act as privileged intermediates for accessing a wide variety of open-chain, carbo- and heterocyclic molecules [1]. On the other hand, they are vital building blocks in many pharmaceuticals as well as natural products that exhibit high biological activity [2]. In the field of coordination chemistry, the ability of β-diketones that are also key structural units of numerous chelating ligands, to form chelate supported coordination compounds with different structures and properties with transition-metal and lanthanide ions has been profusely studied [3-5]. These properties are widely used in the development of extraction methods for the separation of metallic ions with similar properties [6]. Among them, the 4,4,4-trifluoro-1-(2-thienyl)-1,3-butanedione or 2-thenoyltrifluoroacetone (TTA) called our attention owing to its various properties as ionic metal extracting agent [7-9], in the design of luminescent compounds [10], and for its biological activities, for instance, as inhibitor of the mitochondrial electron flux [11]. Moreover, incorporation of thienyl groups in a molecule opens up the opportunity to generate polymeric [12,13] and metallopolymeric materials [14,15], either through chemical or electrochemical oxidation of the thienyl functionality [16-18]. In addition, fluorinated compounds, including those containing the trifluoromethyl moiety, are in general the focus of much interest in modern medicinal chemistry and ideal for use in drug design because of their good biological activity and low toxicity [19-21]. Indeed, the existence of a trifluoromethyl group in a bioactive compound might be expected to induce great changes in molecular properties, such as the hydrophobicity, solubility, special biomimetic effects and electronegativity [22]. Surprisingly, the reactivity of the β-diketones containing thienyl moieties with diamines has been scarcely reported in the literature [23].

In the last few years, we have prepared different kinds of β-diketones [24-26] to be used as precursor for the preparation of several Schiff base ligands [25], metal complexes [27] and Schiff base oligomers [28]. Such condensation reactions proceed via the nucleophilic addition of the primary amine onto the carbonyl carbon giving a hemiaminal -C(OH)(NHR)- intermediate which, depending on the functional groups (R) and the experimental conditions evolves to the formation of a heterocyclic or a polydentate Schiff base compound [29]. Formation of heterocyclic species, namely, 1,4-diazepine and 1,5-benzodiazepine, was indeed observed when 2-thenoyltrifluoroacetone was reacted with 1,2-diaminoethane (en) and 1,2-diaminophenyl, respectively [30], instead of the desired 2-thienyl-containing ONN-tridentate

3

Schif base hemiligands [25,31,32]. Thus, in the quest to prepare thienyl-containing N_2O_2 tetradentate Schiff base compounds, we attempted condensation reactions by using readily available bis[4,4,4-trifluoro-1-(2-thienyl)-1,3-butanedionato]metal (II) [M(TTA)$_2$] metal-chelate templates. A templated reaction of bis(4-amino-3-penten-2-onato)nickel(II) with ethylenediamine has previously been communicated to give the corresponding [Ni(N$_2$O$_2$)] Schiff base complex [33]. In this work, we report on the isolation and full characterization including single crystal X-ray diffraction analysis, of octahedral [M(TTA)$_2$(en)] (M = Co, **2a**; Ni, **2b**; Cu, **2c**) resulting from the coordination of the diamine onto the corresponding starting metal-chelate templates.

2. Experimental

2.1. Materials and physical measurements

Reactions were performed under dry nitrogen or argon atmosphere using standard Schlenk techniques. All starting materials and organic solvents were purchased from commercial sources and used as received. Solid-state FT-IR spectra were recorded on a Bruker IFS28 FTIR infrared spectrophotometer with KBr disks in the 4000 to 400 cm^{-1} range. UV-vis spectra were recorded on an UVIKON XL spectrophotometer. High resolution electrospray ionization mass spectra (ESI-MS) were obtained either with an Agilent 6530 QTOF or a Bruker MAXI 4G mass spectrometer. Elemental analyses were conducted on a Thermo-FINNIGAN Flash EA 1112 CHNS/O analyzer. Cyclic voltammetry (CV) measurements were performed using a CHI604E potentiostat and a standard three-electrode set-up made of a platinum working electrode, a platinum wire auxiliary electrode, and SCE as reference electrode. The system was purged with dinitrogen and maintained under inert atmosphere during the CV experiments. Acetonitrile solutions were 1.0 mM in the compound under study and 0.1 M in the supporting electrolyte n-Bu$_4$N$^+$PF$_6^-$ with voltage scan rate of 100 mVs^{-1}. Ferrocene (Fc) was added as an internal standard at the end of each experiment. The Fc/Fc$^+$ couple was located at $E_{1/2}$ = 0.40 V (ΔE_p = 0.09 V; i$_{pa}$/i$_{pc}$ = 1.0) [34], where $E_{1/2}$ was calculated from the average of the oxidation and reduction peak potentials. Melting points were measured in evacuated capillaries on a Kofler Bristoline melting point apparatus and are uncorrected.

2.2. Synthesis of precursors 1a-c

A Schlenk tube was loaded with a stirring bar, 1.00 g (4.50 mmol) of 2-thenoyltrifluoroacetone and 15 mL of methanol. After 5 min. of stirring, 2.25 mmol (1.0 equiv) of the appropriate hydrated metal acetate salt was added and the reaction mixture was left stirring for 4 h at 20 °C. Then, the solvent was evaporated under reduced pressure. The solid residue was washed with water and filtered off using a glass frit. The collected material was dissolved in CH_2Cl_2 and dried over $MgSO_4$. The solution was filtered off and evaporated to dryness under vacuum.

2.2.1. Complex [Co(TTA)$_2$(CH$_3$OH)$_2$] (1a)

Cobalt(II) acetate tetrahydrate: 0.56 g; light orange solid, 1.13 g (2.00 mmol, 89% yield). m.p. 183-184 °C (dec). Anal. calcd for $C_{18}H_{16}F_6O_6S_2Co$ (565.37 g mol^{-1}): C, 38.24; H, 2.85; S, 11.34. Found: C, 38.39; H, 2.36; S, 12.58. HRMS positive ESI, [m/z] calcd for [$C_{16}H_8O_4F_6S_2{}^{57}Co$]: 500.9100; found: 500.9101 [M]$^+$.

2.2.2. Complex [Ni(TTA)$_2$(H$_2$O)$_2$] (1b)

Nickel(II) acetate tetrahydrate: 0.56 g; light green solid, 1.19 g (2.23 mmol, 99%. yield). m.p. 283-284 °C (dec). Anal. calcd for $C_{16}H_{12}F_6O_6S_2Ni$ (537.08 g mol^{-1}): C, 35.78; H, 2.25; S, 11.94. Found: C, 34.87; H, 2.13; S, 11.73. HRMS positive ESI, [m/z] calcd for [$C_{16}H_8O_4F_6S_2{}^{58}Ni$]: 501.9076; found: 501.9098 [M]$^+$.

2.2.3. Complex [Cu(TTA)$_2$] (1c)

Copper(II) acetate monohydrate: 0.45 g; light green solid, 1.19 g (2.10 mmol, 93%. yield). m.p. 220 °C (dec). Anal. calcd for $C_{16}H_8F_6O_4S_2Cu$ (504.91 g mol^{-1}): C, 37.99; H, 1.59; S, 12.68. Found: C, 38.33; H, 1.64; S, 13.34. HRMS positive ESI, [m/z] calcd for [$C_{16}H_8F_6O_4S_2{}^{63}Cu$]: 504.9064; found: 504.9075 [M]$^+$.

2.3. Synthesis of complexes 2a-c

A Schlenk tube was loaded with a stirring bar, the desired precursor **1a-c** and 15 mL of methanol. After 5 min. of stirring, ethylendiamine was added dropwise and the reaction mixture was stirred for 4 h at 20 °C. Then, the resulting solution was evaporated under reduced pressure and the solid residue was washed with water and filtered off using a glass frit. The collected material was dissolved in CH_2Cl_2 and dried over $MgSO_4$. The solution was filtered off and evaporated to dryness under vacuum.

2.3.1. Complex [Co(TTA)₂(en)] (2a)

Precursor **1a**: 1.00 g (1.78 mmol), ethylenediamine: 0.12 mL (1.78 mmol); orange solid, 0.93 g (1.65 mmol, 93%. yield). Slow evaporation of an ethanol solution gave single crystals that were used for X-ray diffraction analysis. m.p. 223 °C (dec). Anal. Calcd for $C_{18}H_{16}CoF_6N_2O_4S_2$ (561.38 g mol^{-1}): C, 38.51; H, 2.87; N, 4.99; S, 11.42. Found: C, 38.53; H, 2.92; N, 5.63; S, 10.97. HRMS positive ESI, [*m/z*] calcd for $[C_{18}H_{16}N_2O_4F_6S_2{}^{57}Co+Na]$: 560.97820; found: 560.97820 [M]$^+$. FT-IR (KBr, cm^{-1}): 3210(s), 3112(s) ν(N-H); 2962(w) ν(C-H arom); 2854(w) ν(C-H aliph); 1618(vs) ν(C=O); 1528 (vs) ν(C=C); 1138(vs) ν(C-N); 716 (s) δ(C-H C_4H_3S).

2.3.2. Complex [Ni(TTA)₂(en)] (2b)

Precursor **1b**: 1.00 g (1.86 mmol), ethylenediamine: 0.13 mL (1.95 mmol); green solid, 0.95 g (1.70 mmol, 96% yield). Slow evaporation of an ethanol solution gave single crystals that were used for X-ray diffraction analysis. m.p. 265 °C (dec). Anal. Calcd for $C_{18}H_{16}O_4N_2F_6S_2Ni$ (561.14 g mol^{-1}): C, 38.53; H, 2.87; N, 4.99; S, 11.43. Found: C, 38.30; H, 2.99; N, 4.49; S, 10.95. HRMS positive ESI, [*m/z*] calcd for $[C_{18}H_{16}N_2O_4F_6S_2{}^{58}Ni+Na]$: 582.97010; found: 582.97150 [M + Na]$^+$. FT-IR (KBr, cm^{-1}): 3363, 3285(w) ν(N-H); 3172(w) ν(C-H arom); 2964(w) ν(C-H aliph); 1596(vs) ν(C=O); 1534 (vs) ν(C=C); 1131(vs) ν(C-N); 715 (vs) δ(C-H C_4H_3S).

2.3.3. Complex [Cu(TTA)₂(en)] (2c)

Precursor **1c**: 1.00 g (1.98 mmol), ethylenediamine: 0.14 mL (2.10 mmol); green solid, 0.93 g (1.65 mmol, 83% yield). Slow evaporation of an ethanol solution gave single crystals that were used for X-ray diffraction analysis. m.P. 152-153 °C (dec). Anal. Calcd for $C_{18}H_{16}CuF_6N_2O_4S_2$ (566.00 g mol^{-1}): C, 38.20; H, 2.85; N, 4.95; S, 11.33. Found: C, 38.11;

H, 2.39; N, 4.61; S, 11.47. HRMS positive ESI, [*m/z*] calcd for $[C_{16}H_8O_4F_6NaS_2{}^{63}Cu+Na]$: 527.89564; found: 527.8960 $[Cu(TTA)_2+Na]^+$; [*m/z*] calcd for $[C_{10}H_{12}N_2O_2F_3S{}^{63}Cu+H]$: 343.98621, found: 343.9863 $[Cu(TTA))(en+H]^+$. FT-IR (KBr, cm^{-1}): 3299 (m), 3235 ν(N-H); 3172(w) ν(C-H arom); 2963 (w), 2952(w), 2888(w) ν(C-H aliph); 1621(vs) ν(C=O); 1497 (vs) ν(C=C) 1106(vs) ν(C-N); 706 (s) δ(C-H C$_4$H$_3$S).

2.4. X-ray Crystal Structure Determinations

A crystal of appropriate size and shape of each of the compounds **2a**, **2b** and **2c** was coated with Paratone-N oil, mounted on a cryoloop and transferred to the cold gas stream of a cooling device. Intensity data were recorded at T = 150(2) K on a Bruker APEXII AXS diffractometer using Mo- Kα radiation (λ = 0.71073 Å), equipped with a bidimensional CCD detector, and were corrected for absorption effects using multiscanned reflections. All the structures were solved by direct methods using the SIR97 program [35] and then refined using full-matrix least-squares methods based on F2 (SHELXL-97) [36]. The disorder observed for the carbon and sulfur atoms of the thiophene fragment in the three compounds was modelled using two positions per carbon and sulfur atom with fixed occupancy factors of 0.70/0.30 and 0.52/0.48 in **2a**, 0.47/0.53 in **2b**, and 0.83/0.17 in **2c**. All nonhydrogen atoms were refined with anisotropic atomic displacement parameters. All hydrogen atoms were placed at their geometrically idealized positions and constrained to ride on their parent atoms, except for the nitrogen-linked hydrogen atoms, in **2b** and **2c**, which were introduced in the structural model through Fourier difference maps analysis and refined. A summary of the details of the data collection and refinement for the X-ray structures of the three compounds is given in Table 1, and additional crystallographic details are in the CIF file. ORTEP views were drawn using OLEX2 software [37].

Table 1. Crystallographic data, details of data collection and structure refinement parameters for compounds **2a**, **2b** and **2c**

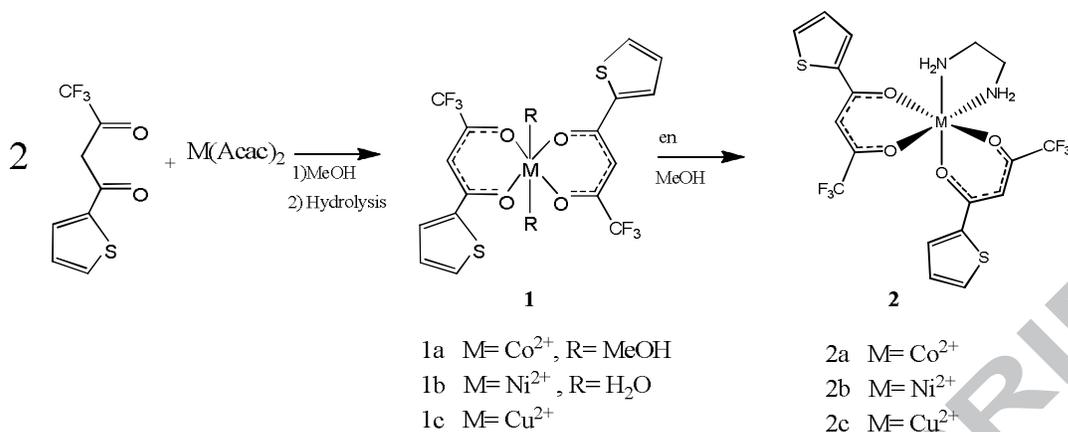|	2a	2b	2c
Empirical Formula	$C_{18}H_{16}CoF_6N_2O_4S_2$	$C_{18}H_{16}F_6N_2\ NiO_4S_2$	$C_{18}H_{16}CuF_6N_2O_4S_2$
Formula mass, g mol^{-1}	561.38	561.16	565.99
Collection T, K	150(2)	150(2)	150(2)
Crystal size (mm)	0.28 x 0.10 x 0.06	0.54 x 0.11 x 0.07	0.44 x 0.14 x 0.07
Crystal color	Orange	Yellow	Green
Crystal system	Triclinic	Monoclinic	Triclinic
Space group	P-1	$C1_2/c1$	P-1
a (Å)	10.407(3)	22.493(3)	10.2720(6)
b (Å)	10.494(4)	10.5241(14)	10.4045(6)
c (Å)	12.501(4)	10.4126(14)	11.8161(6)
α (°)	115.253(18)	90	111.194(2)
β (°)	108.507(16)	111.136(5)	101.940(2)
γ (°)	92.12(2)	90	96.814(2)
V (Å^3)	1147.0(7)	2299.0(5)	1125.75(11)
Z	2	4	2
D_{calcd} (g cm^{-3})	1.625	1.621	1.670
$F(000)$	566	1136	570
abs coeff (mm^{-1})	1.006	1.101	1.233
θ range (°)	3.198 to 26.914	3.249 to 27.463	3.011 to 27.414
range h,k,l	-12/13, -13/12, -15/15	-29/20, -9/13, -12/13	-13/13, -13/12, -14/15
No. total refl.	13791	7666	15270
No. unique refl.	13791	2616	5030
Comp. to θ_{max} (%)	93.6	99.2	97.9
Max/min transmission	0.941/0.635	0.926/0.724	0.917/0.833
Data/Restraints/Parameters	13791/0/301	2616/0/157	5030/6/303
Final R	$R_1 = 0.0866$	$R_1 = 0.0513$	$R_1 = 0.0559$
[$I>2\sigma(I)$]	$wR_2 = 0.2133$	$wR_2 = 0.1208$	$wR_2 = 0.1378$
R indices (all data)	$R_1 = 0.1487$	$R_1 = 0.0974$	$R_1 = 0.0783$
	$wR_2 = 0.2698$	$wR_2 = 0.1416$	$wR_2 = 0.1487$
Goodness of fit / F^2	0.979	1.005	1.081
Largest diff. Peak/hole (eÅ^{-3})	1.207/-1.041	0.362/-0.587	1.308/-0.760

2.5. Computational details

Density functional theory (DFT) calculations were carried out using the ADF2013 package [38], employing the PW91 functional [39] and the TZ2P basis set [40]. Spin-unrestricted calculations were carried out on all the open-shell systems. The geometry optimizations were carried out assuming the X-ray structures as input data, without any symmetry constraint. Nevertheless, in the case of **2a** and **2b** the converged geometries were found to be of C_2 symmetry. The optimized geometries were characterized as true minima on the potential energy surface using vibration frequency calculations (no imaginary values). The UV-vis transitions were calculated by means of TDDFT calculations [41] on the optimized geometries, at the same level of theory.

3. Results and discussion

3.1. Synthesis and characterisation of the complexes

The known precursors $[Co(TTA)_2(CH_3OH)_2)]$ (**1a**) [42], $[Ni(TTA)_2(H_2O)_2]$ (**1b**) [43], and $[Cu(TTA)_2]$ (**1c**) [43,44] were prepared using slightly modified synthetic procedures in order to improve their corresponding yields. Compounds **1a-c** were, indeed, readily isolated in almost quantitative yields (89-99%) upon mixing 2-thenoyltrifluoroacetone with the appropriate hydrated metal(II) acetate salt in ethanol for 4 h at room temperature. Analytical data were in accord with reported ones [42-44] and with their chemical compositions (see section 2.2).

We then attempted the condensation reactions between the precursor compounds **1a-c** and 1,2-diaminoethane in order to synthetize directly the respective symmetrical $[M(N_2O_2)]$-type Schiff base complexes. Whatever the experimental conditions used (refluxing methanol and ethanol, refluxing toluene assisted with Dean-Stark trap to remove formed water, in the presence or absence of catalytic amount of acetic acid) the octahedral products $[M(TTA)_2(en)]$ (M = Co, **2a**; Ni, **2b**; Cu, **2c**) were always isolated in modest to reasonable yields. The one-pot reaction involving the metal-acetate salts and stoechiometric mixture of TTAH and en lead also to the formation of compounds **2a-c** in poor yields. Finally, **2a-c** were isolated in high yields (83-96%) by simply mixing precursors **1a-c** and en in ethanol at room temperature for 4 h (Scheme 1). Complexes **2a-c** are air and thermally stable, and exhibit good solubility in solvents such as CH_2Cl_2, THF, MeOH, EtOH, toluene, DMF and acetonitrile. Their composition and structures were established by satisfactory elemental analyses, absorption spectroscopy and mass spectrometry (see section 2.3). Furthermore, the molecular and crystal structures of the three compounds were determined by single crystal X-ray diffraction (see section 3.2).

Scheme 1 Synthesis of the octahedral complexes **2a-c**

High resolution ESI$^+$ mass spectra of **2a** and **2b** showed the molecular ion peaks at M/z= 560.97820 [M]$^+$ and 582.97010 [M + Na]$^+$ that matched the calculated values of 560.97820 and 582.97150, respectively. ESI-MS of **2c** did not give the parent molecular ion peaks. Nevertheless, prominent fragment ions are observed at M/z= 527.89564 assigned to [^{63}Cu(TTA)$_2$ + Na]$^+$ and at M/z= 343.98621 attributed to [(^{63}Cu(TTA)(en) + H]$^+$. For all these peaks, the envelope of the isotopic pattern was in good agreement with the simulated ones.

Solid-state FT-IR spectra of compounds **2a-c** exhibit similar profiles suggesting similar organization of ligands about the metal center. The double band pattern at 3400 and 3100 cm^{-1} is assigned to the asymmetric and symmetric -NH$_2$ stretching vibrations, respectively. Two prominent absorptions around 1600 and 1500 cm^{-1} (see section 2.3 for details) are due to v(C=O) and v(C=C) stretching modes of the chelate rings, the latter including also the thienyl ring stretches and the δ(NH$_2$) deformation mode [25, 32]. Those intense bands are typical for metal β-diketonate complexes [42-44, 45]. The band between 1140 and 1100 cm^{-1} is attributed to the C-N bond vibration of the ethylenediamine ligand. Finally, the strong absorption band observed about 710 cm^{-1} is due to the δ(C-H) out-of-plane bending mode of the 2-thienyl group [46].

3.2. X-ray Crystallographic Studies

Complexes **2a**, **2b** and **2c** were crystallized by slow evaporation of ethanolic solutions as orange, yellow and green rectangular-shaped crystals, respectively. Both cobalt (**2a**) and copper (**2c**) complexes are arranged in a triclinic crystal system in the centrosymmetric space

group P-1, with a single molecule in the asymmetric unit. The nickel complex **2b** crystallizes in the monoclinic centrosymmetric space groups $C1_2/c1$ with a half molecule in the asymmetric unit. The molecular structures of **2a**, **2b** and **2c** with partial atom labeling scheme are displayed in Fig. 1.
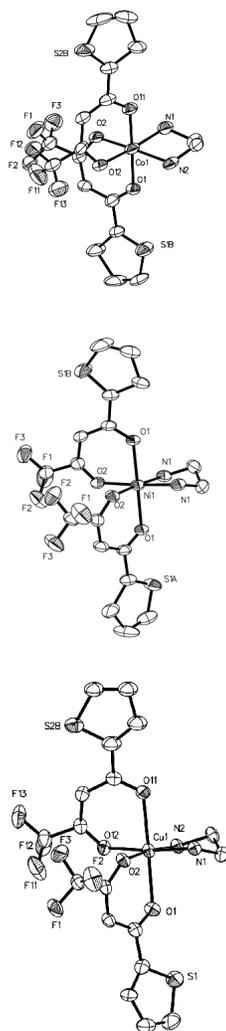

Fig. 1 Molecular structures of **2a** (top), **2b** (middle) and **2c** (bottom) with partial atom labeling scheme. Hydrogen atoms have been omitted for clarity. Thermal ellipsoids are drawn at 50% probability.

Selected bond lengths and angles for **2a** and **2c** are provided in Table 2 (their atom labeling is the same). Those of **2b** are given in Table 3. Other selected metrical data for **2a** and **2c** are provided in Table S1. In the three compounds, the metal is ligated to a couple of monoanionic 2-thenoyltrifluoroacetonato chelates and to a neutral ethylenediamine molecule,

11

forming the $[N_2O_4]^{2-}$ donor set of atoms. The three complexes adopt a distorted octahedral coordination sphere at the metal(II) centers that manifests itself by a slight departure from linearity of the *trans* bond angles O-M-X (X = O, N), and significant variations in the *cis* bond angles (Tables 2 and 3).

According to Jahn-Teller effect [47] in d^7 cobalt(II) and d^9 copper(II) electronic configurations, the coordination sphere at the metal(II) ion is expected to be elongated (or contracted) along one of the three L-M-L axis of the octahedral core [48]. Compound **2a** appears to be very slightly elongated along the O(12)-Co(1)-N(1) axis (Fig. 1), with the Co(1)-O(12) bond length (2.111(5) Å) longer by 0.04 Å than the other Co-O bond distances (average: 2.072 Å) and the axial Co(1)-N(1) bond length larger by 0.04 Å than the equatorial Co(1)-N(2) one (Table 2). The arrangement of donor atoms around the central Cu(II) metal ion is somewhat different in **2c**, since the elongation occurs along the O(1)-Cu(1)-O(11) axis (Fig. 1). Here, the elongation is much greater with the axial Cu-O bond lengths longer by 0.311 Å in average than their equatorial Cu-O counterparts (Table 2).

Table 2 X-ray bond distances (Å) and angles (°) of the octahedral skeleton in compounds **2a** and **2c**. Corresponding DFT-optimized values are given into brackets.

	2a	2c
	Bond distances	
M(1)-O(1)	2.074(6) [2.157]	2.292(3) [2.336]
M(1)-O(2)	2.064(5) [1.929]	1.976(3) [2.004]
M(1)-O(11)	2.077(6) [2.157]	2.297(3) [2.337]
M(1)-O(12)	2.111(5) [1.929]	1.991(3) [2.005]
M(1)-N(1)	2.148(7) [2.014]	2.018(3) [2.117]
M(1)-N(2)	2.107(6) [2.014]	2.022(4) [2.117]
	Bond angles	
O(1)-M(1)-O(11)	178.6(2) [171]	178.13(11) [167]
O(2)-M(1)-N(2)	172.8(2) [176]	173.40(14) [168]
O(12)-M(1)-N(1)	173.7(3) [178]	174.20(14) [168]
O(1)-M(1)-O(2)	87.0(2) [93]	86.23(11) [98]
O(1)-M(1)-O(12)	92.3(2) [93]	93.59(12) [101]
O(1)-M(1)-N(1)	87.5(3) [89]	91.95(13) [88]
O(1)-M(1)-N(2)	87.4(2) [89]	87.68(13) [81]
O(2)-M(1)-O(11)	92.6(2) [93]	92.06(12) [101]
O(2)-M(1)-O(12)	86.9(2) [92]	89.61(12) [96]
O(2)-M(1)-N(1)	94.8(2) [92]	92.50(13) [92]
O(11)-M(1)-O(12)	86.3(2) [93]	85.64(11) [88]
O(11)-M(1)-N(1)	87.5(3) [84]	88.88(13) [81]
O(11)-M(1)-N(2)	93.1(2) [92]	94.06(14) [92]
O(12)-M(1)-N(2)	97.8(2) [92]	93.32(13) [88]
N(1)-M(1)-N(2)	81.2(2) [85]	85.16(14) [82]

M = Co, **2a**; Cu, **2c**.

As in **2a** and **2c** the M(II) center does not reside on a crystallographic inversion center, the *trans* O-M-O and O-M-N angles deviate slightly more from linearity compared to the nickel analogue **2b** (see below). They indeed vary between 172.8(2)° and 178.6(2)° (Table 2). The O-M-O bite angles are found in the narrow range 85.64(11) - 87.0(2)° (Table 2), while the N-M-N bite angles are of 81.2(2)° for **2a** and 85.16(14)° for **2c**.

The nickel complex **2b** crystallizes with the Ni(II) metal ion occupying a crystallographic inversion center and is coordinated by a nearly octahedral geometry of four oxygen and two nitrogen atoms (Fig. 1). The O-Ni-O and O-Ni-N diagonal angles are equal to 179.29(14)° and 176.79(11)°, respectively. Coordination of the β-diketonate and diamine ligands in a bidentate fashion forms two six- and one five-membered rings with O-Ni -O and N-Ni-N bite angles of 88.17(9)° and 83.79(17)°, respectively. The two almost identical Ni-O and the Ni-N bond lengths (Table 3) are similar to those reported for octahedral Ni(TTA)$_2$(N-N) species [43].

Table 3 Selected X-ray bond distances (Å) and angles (°) for compound **2b.** with their corresponding DFT-optimized values given into brackets

Bond distances			
Ni(1)-O(1)	2.050(2) [2.058]	Ni(1)-N(1)	2.075(3) [2.154]
Ni(1)-O(2)	2.058(2) [2.043]	O(1)-C(5)	1.262(4) [1.275]
O(2)-C(7)	1.271(4) [1.266]	C(5)-C(6)	1.422(5) [1.419]
C(6)-C(7)	1.388(5) [1.394]	N(1)-C(9)	1.470(5) [1.472]
C(9)-C(9)[#1]	1.518(7) [1.526]		
Bond angles			
O(1)-Ni(1)-O(1)[#1]	179.29(14) [173]	O(2)-Ni(1)-N(1)	176.79(11) [173]
O(1)-Ni(1)-O(2)	88.17(9) [92]	O(1)-Ni(1)-N(1)	88.94(11) [90]
O(1)-Ni(1)-O(2)[#1]	91.32(9) [93]	O(1)-Ni(1)-N(1)[#1]	91.59(11) [90]
O(2)-Ni(1)-N(1)[#1]	94.90(11) [92]	O(2)-Ni(1)-O(2)[#1]	86.55(13) [95]
N(1)-Ni(1)-N(1)[#1]	83.79(17) [81]	C(5)-C(6)-C(7)	122.9(3) [125]
Ni(1)-O(1)-C(5)	126.1(2) [125]	Ni(1)-O(2)-C(7)	121.2(2) [122]
O(1)-C(5)-C(6)	125.2(3) [125]	O(2)-C(7)-C(6)	129.2(4) [130]
Ni(1)-N(1)-C(9)	107.5(2) [108]		

Symmetry code: #1 -x, y, -z+1/2

Concerning the 2-thenoyltrifluoroacetonato ligand and whatever the complex **2a**, **2b** or **2c** (see Tables 2 and S1), the C-O bonds adjacent to the thienyl (Th) substituent is slightly

shorter compared to that of the CF_3-substituted side. The opposite trend is observed for the β-diketonato carbon backbone where the C-C(Th) bond is slightly longer than the C-C(CF$_3$) bond. Both bonds exhibit double bond character, typical of β-diketonato ligands [49]. Due to this slight asymmetry in bond lengths, the associated bond angles are affected, with the O-C(CF$_3$)-C angles about 4-6° larger than the O-C(Th)-C angles. There is not rotational disorder associated with the CF$_3$ groups, so all the C-F bond distances are quite similar. On average, the C-F bond lengths are of 1.328 Å in **2a**, 1.333 Å in **2b**, and 1.334 Å in **2c**. On the other hand, the two thiophene rings of **2a**, that of **2b**, and one thiophene ring of **2c** show statistical disorder involving a 180° rotation of the ring around the C(4)-C(5) and C(14)-C(15) bonds, so that S(1A)/S(2A) and S(1B)/S(2B) are composite S/C sites (see the cif files in SI). Orientational disorder of thiophene rings over two positions is quite common [50,51]. The thiophene rings are planar within experimental error and coplanar with their respective attached methallacycles, making dihedral angles of 3.2° and 7.5° in **2a**, 1.9° in **2b**, and 17.8° and 5.5° in **2c**. Their bond lengths and angles as well as those of the ethylenediamine ligands are unexceptional [52].

Finally, within the crystal structures of **2a-c** there is a number of intermolecular hydrogen bond interactions of the type N-H⋯O that creates, in each case, a chain structure in the packing (Fig. S1 and Table S2).

3.3. Electronic absorption spectra

The electronic absorption spectra of complexes **2a-c** were recorded at room temperature in 10^{-3} M and 10^{-6} M ethanol solutions in the ranges 450-900 nm and 250-450 nm, respectively. The UV and visible spectra are shown in Fig. 2 and the experimental and computed electronic spectral data are presented in Table 4. The electronic spectra of complexes **2a-c** are very similar to each other and consist of one very intense broad band in the region of 250 to 400 nm, on grounds of TDDFT study attributed to an intraligand π-π* charge transfer (LLCT) transition, and a low-energy absorption band from 450-900 nm region presumably involving frontier orbitals (Table 4 and Section 3.5) [43,53,54].
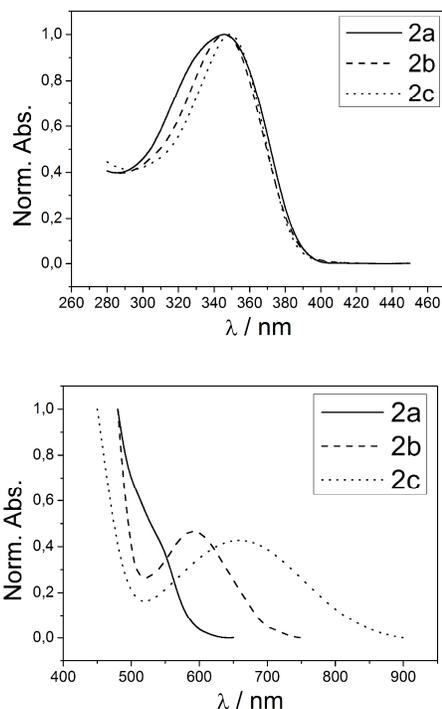
14

Fig. 2 UV spectra (top) and Vis spectra (bottom) measured in ethanol for complexes **2a** (solid line), **2b** (dashed line) and **2c** (dotted line).

Table 4 Experimental and computed electronic spectral data for compounds **2a-c**. Wavelengths are expressed in nm.

2a		2b		2c	
Exp.[a]	Calc.	Exp.[a]	Calc.	Exp.[a]	Calc.
λ_{max} (log ε)	λ (o.s.)[b]	λ_{max} (log ε)	λ (o.s.)[b]	λ_{max} (log ε)	λ (o.s.)[b]
		346 (5.20)	335 (0.12)		300 (0.17)
			343 (0.19)	349 (5.80)	331 (0.12)
	345 (0.14)		364 (0.13)		350 (0.13)
346 (5.30)	345 (0.11)		370 (0.11)		413 (0.12)
	LLCT		MLCT		LLCT (maj.)

15

			423 (0.02)		480 (0.01)
			LLCT		495 (0.01)
					497 (0.01)
					MLCT (maj.)
	538 (0.04)	591 (1.47)	503 (0.03)	634 (2.06)	612 (0.02)
537 (1.60)	540 (0.05)		MLCT		LMCT
	MLCT				

[a] Values recorded in ethanol. [b] Major computed transition wavelengths contributing to the band, with corresponding oscillator strengths in parenthesis.

3.4. Electrochemical study

The electrochemical oxidation of complexes **2a-c** was investigated by cyclic voltammetry (CV) in acetonitrile solutions, at 293 K, in the potential range -0.5 to +2.0 V versus SCE reference electrode. The three complexes present a similar potentiodynamic behavior where the stabilized profile exhibits two irreversible anodic waves (Fig. 3). The first peaks are located at 0.80, 0.70 and 0.60 V whereas the second oxidation waves appeared at 1.35, 1.16 and 1.00 V/SCE for **2a**, **2b** and **2c**, respectively. From our DFT calculations (see below), the first peaks could be assigned to the M(II)/M(III) redox couples, while the second ones could result from the oxidation of soluble dimeric or short oligomeric species generated during the first redox event. The fact that the second wave of **2c** is more intense than that observed for its **2a** and **2b** counterparts (Fig. 3) might be due to faster follow up reaction of the mono-oxidized species **2c⁺**, owing to a greater delocalization of the spin density on the ligands (see Section 3.5). In any case we have noted deposits of polymeric species on the electrode surface. This lack of massive deposit of polymer could be attributed to either the weak contribution of the 2-thienyl group to the spin density or to the electron-attracting effect of the CF_3 moieties that limits the extension of the electropolimerization and does only allow the formation of soluble short oligomers with low molecular weight. Very recently, we have shown that when the CF_3 substituent is absent in the thienyl-containing β-diketonate structure, polymeric massive deposits can be obtained on the electrode surface [55].
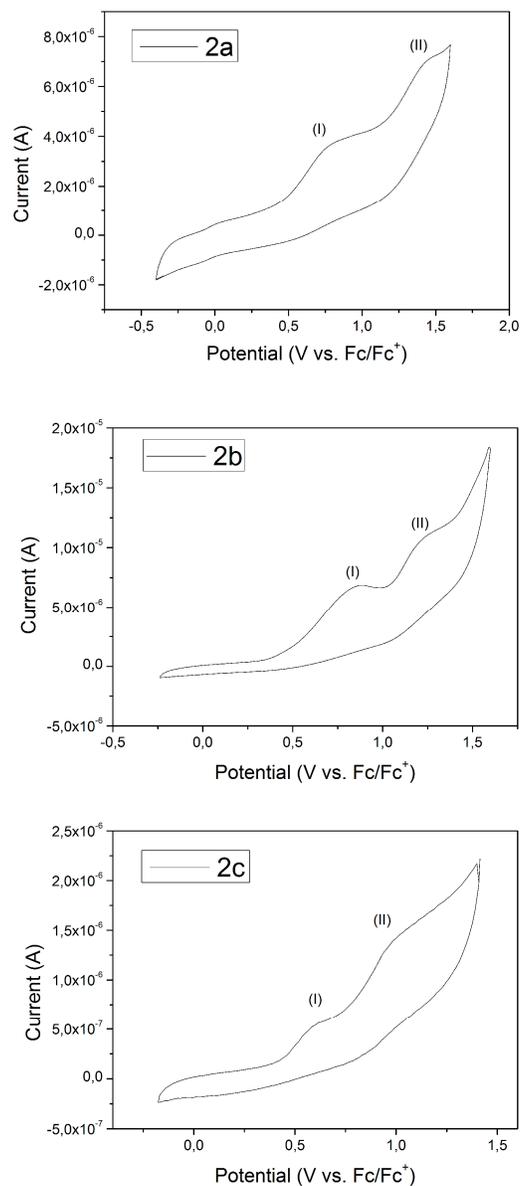
Fig. 3. Cyclic voltammograms of complexes **2a** (top), **2b** (middle) and **2c** (bottom) recorded in acetonitrile containing 0.1 M n-Bu$_4$N$^+$PF$_6^-$ at T=293 K with a sweep rate v = 0.1 Vs^{-1} and SCE as reference electrode. Potentials are referenced to the Fc/Fc$^+$ couple at +0.40 V vs. SCE [34].

3.5. Theoretical investigations

In order to get a better insight into the bonding and properties of compounds **2a-c**, we have carried out DFT calculations on these compounds. Details of the calculations are given in section 2.5. Their fully optimized geometries were characterized as true energy minima by vibrational frequency calculations. Those of 2a and 2b were found to be of C_2 symmetry, whereas that of **2c** was found to be very close to C_2, with the C_2 axis bisecting the N-M-N angle. Selected metrical data are given in Tables 2 and 3. They are in a good overall agreement with the X-ray structures. The MO diagrams of **2a-c** are shown in Figs. 4-6, respectively. Due to the spin-unrestricted nature of the calculations, each MO level in these diagrams is split into two spinorbitals: one spin-up (left) and one spin-down (right). **2a**, **2b** and **2c** are 19-, 20- and 21-electron pseudo-octahedral transition-metal complexes, respectively. Thus, their 3d atomic shell generates in the complexes a set of five metal-based MOs which are split in a fully occupied "t_{2g}" set and an antibonding "e_g" set which contains 1, 2 and 3 electrons in **2a**, **2b** and **2c**, respectively. In the three complexes, the occupied "t_{2g}" orbitals are rather low-lying. In the case of **2a**, the unpaired "e_g" electron lies in a d_{z2}-based orbital, the z axis being defined by O(11), Co(1) and O(1) (see Fig. 1). In **2b**, the two "e_g" electrons are unpaired and occupy d_{z2}- and d_{x2-y2}-based orbitals, z being the O(1)-Ni(1)-O(1)[#] axis. In **2c**, the three "e_g" electrons adopt the $(d_{z2})^2 (d_{x2-y2})^1$ configuration, z being defined as in **2a**. The Jahn-Teller distortion in **2a** and **2c**, associated with a larger occupation of the d_{z2}-type MO with respect to that of its d_{x2-y2} counterpart, is found to be an elongation along the z, *i.e.* O(11)-M(1)-O(11), axis. This finding is fully consistent with the X-ray structure of **2c**, but not with that of **2a**, which exhibits a barely significant distortion along its O(12)-Co(1)-N(2) axis (see Section 3.2). We suggest the computed Jahn-Teller effect in **2a** too weak for being observed in its actual X-ray structure, being cancelled by packing forces. The spin densities of **2a**, **2b** and **2c**, plotted in Fig. 7, reflect their electron configuration. The computed Mulliken metal spin densities are 0.95, 1.52 and 0.53 for **2a**, **2b** and **2c**, respectively. The rather low value of **2c** (as compared to **2a** for example) indicates a larger delocalization of the spin density on the ligands (in particular on the nitrogen atoms).
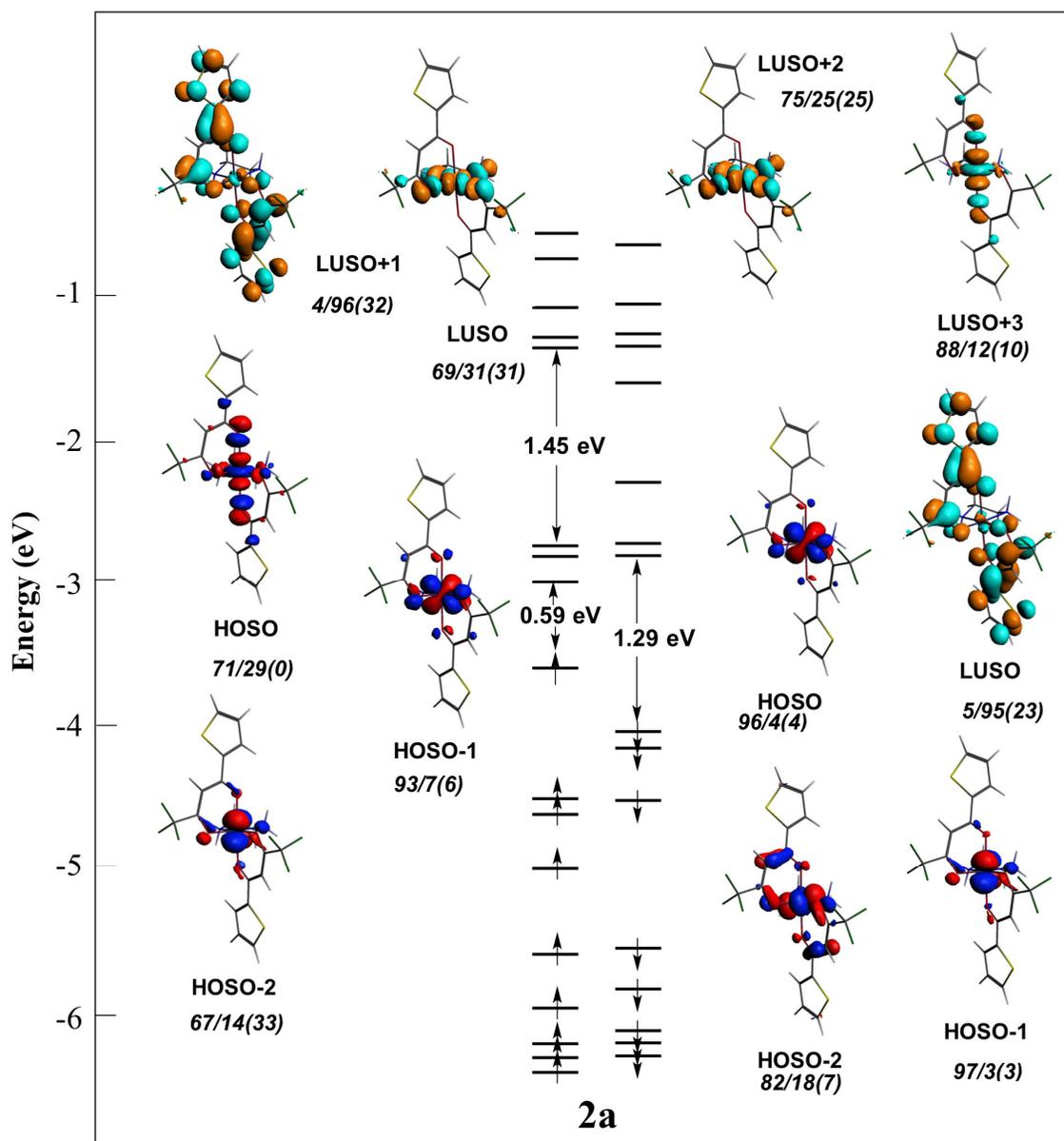
18

Fig. 4 Kohn-Sham spin-orbital level ordering of **2a**. The localizations (in %) are given in the following order: metal/ligand(coordinated heteroatoms). HOSO: highest occupied spin-orbital; LUSO: lowest unoccupied spin-orbital.
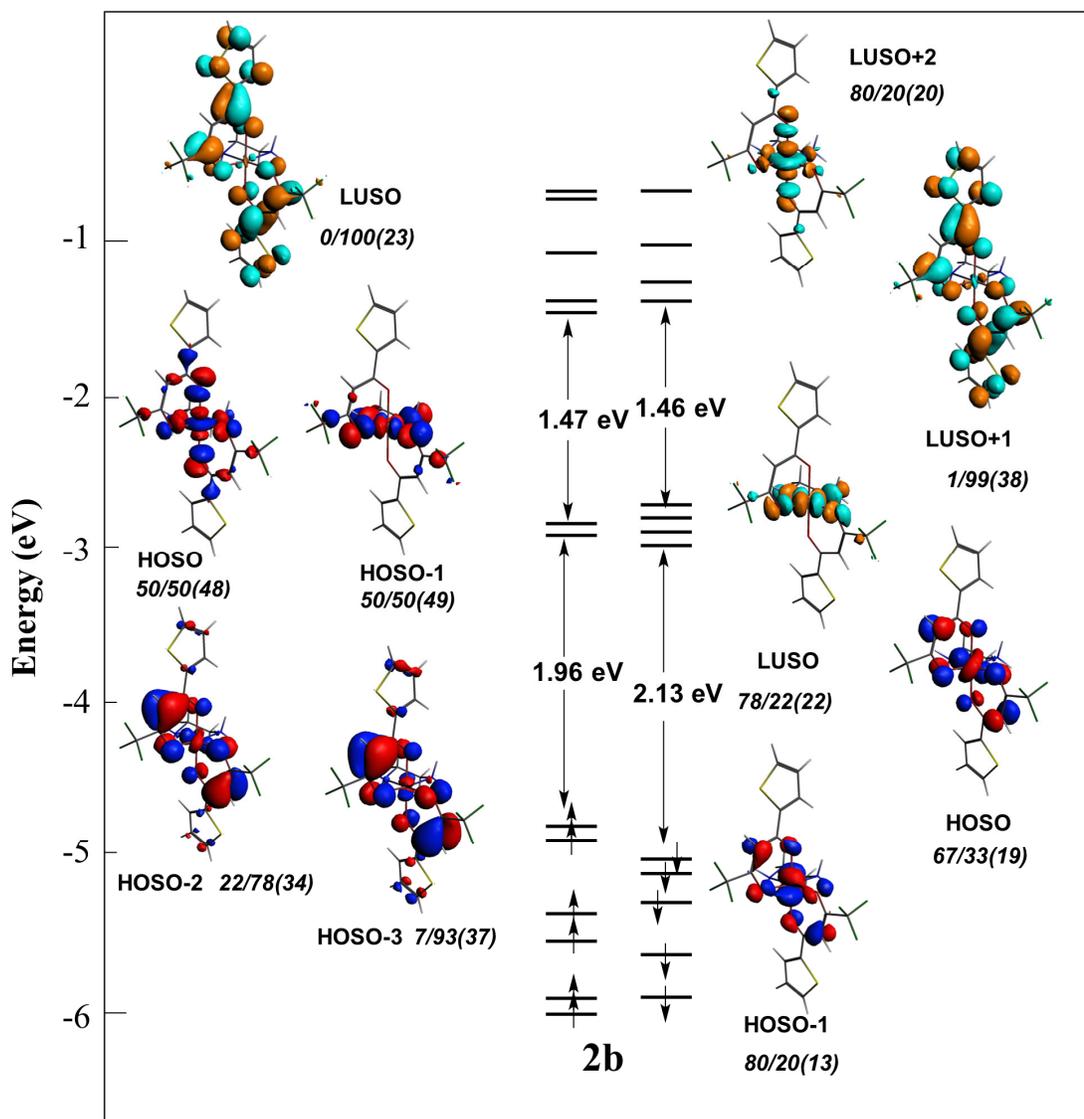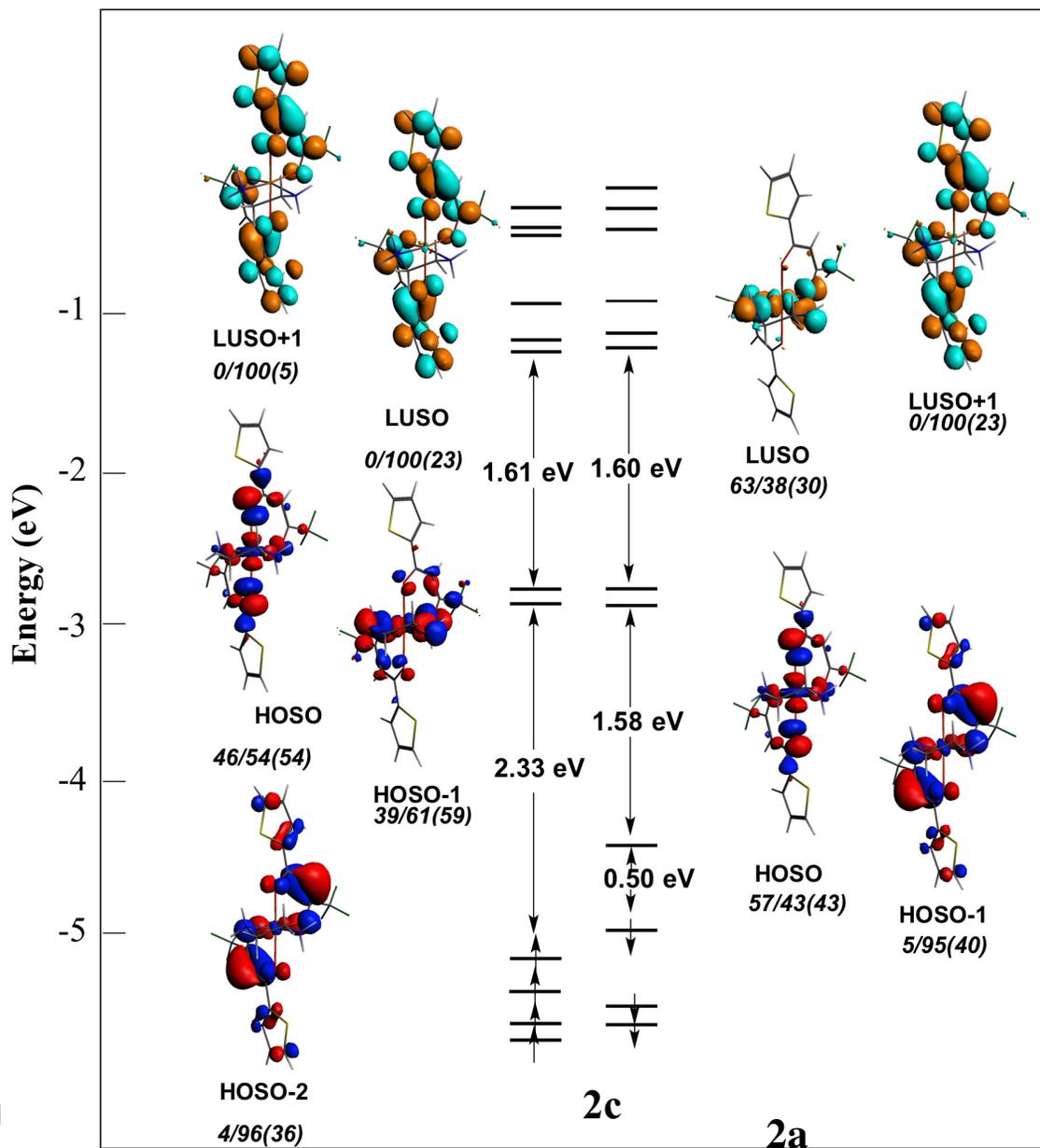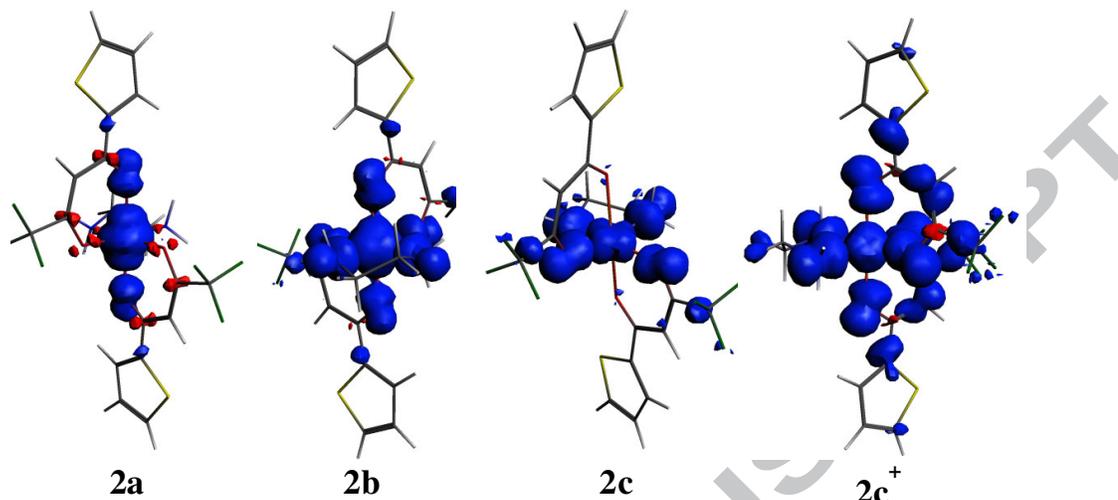
Fig. 5 Kohn-Sham spin-orbital level ordering of **2b**. The localizations (in %) are given in the following order: metal/ligand(coordinated heteroatoms). HOSO: highest occupied spin-orbital; LUSO: lowest unoccupied spin-orbital.

Fig. 6 Kohn-Sham spin-orbital level ordering of **2c**. The localizations (in %) are given in the following order: metal/ligand(coordinated heteroatoms). HOSO: highest occupied spin-orbital; LUSO: lowest unoccupied spin-orbital.

Fig. 7 Spin density plots of compounds **2a**, **2b**, **2c** and **2c⁺**.

For a better understanding of the electrochemical behavior of **2a**-**c**, their mono-oxidized forms have been also computed, in a similar way as their neutral counterparts. The ground state of **2a⁺** is found to be a singlet (HOMO-LUMO gap = 1.84 eV) with the electron configuration of a regular octahedral 18-electron complex. The ground state of **2b⁺** is a doublet, with an electron configuration similar to that of the isoelectronic neutral **2a**. Consistently, the Mulliken Ni spin density is 0.71, *i.e.* about half of that in neutral **2b**. As for its isoelectronic **2b** relative, **2c⁺** is found to have a triplet ground state and has the same $(d_{z2})^1$ $(d_{x2-y2})^1$ configuration. However, the occupied "e_g" spinorbitals of **2c⁺** have a much larger ligand character than those of **2b**. It results that the spin density of **2c⁺** (see Fig. 7) has a similar general shape as that of **2b**, but it is much more delocalized on the ligands. As a result, the Mulliken metal spin density is only 0.68, whereas the major ligand contributions involve the six donor atoms bonded to the metal (Fig. 1), *i.e.*, N (0.14), O(1) (0.18) and O(2) (0.32). However, the contribution of the 2-thienyl heterocycle to the spin density remains weak.

22

The TDDFT-computed UV-visible transitions corresponding to the major optical transitions for **2a-c** are reported in Table 4. Owing to the open-shell configurations of the three complexes and to our level of calculations, the agreement is expected to be only qualitative, but allows indexing the main features of the experimental spectra. In the case of **2a**, the agreement is in fact very good. The high-energy band is due to LLCT (intraligand π-π^*) transitions and the low-energy one is associated with $M(t_{2g})$-to-ligand transitions. In the case of **2b** and **2c** an intermediate band (not experimentally observed) is computed near 420 and 490 nm, respectively. The strong bands at high energy of **2b** and **2c** are of MLCT and LLCT character respectively. In the case of **2c**, it has some minor MLCT contribution. The low-energy band is of major MLCT and LMCT character for **2b** and **2c**, respectively. It is noteworthy that for the three compounds no transition with large d-d character could be identified, but only minor contributions to the bands of lower energy. This may be related to the electron richness of the compounds and to the presence of low-lying vacant ligand orbitals (Figures 4-6).

4. Conclusion

To sum up, attempted condensation reactions of bis(2-thenoyltrifluoroacetonato) metal-chelate templates $[Co(TTA)_2(CH_3OH)_2]$, $[Ni(TTA)_2(H_2O)_2]$ and $[Cu(TTA)_2]$ with 1,2-diaminoethane lead in each case to the formation of their corresponding octahedral bis(β-diketonate)-ethylenediamine metal(II) complexes $[M(TTA)_2(en)]$. These six-coordinate paramagnetic compounds were fully characterized by analytical and spectroscopic methods, as well as by single-crystal X-ray diffraction study. Their electronic structure and properties have been analysed by DFT and TDDFT calculations. Each metal ion adopts a distorted octahedral geometry; the Cu(II) derivative showing a significant elongation along the O-Cu-O axis due to Jahn-Teller distortion associated with the "e_g" electron occupation of the d_{z2}-type MO. Cyclic voltamograms in the anodic region show two irreversible oxidation waves. Our DFT calculations indicate that the first wave is associated with the oxidation of the metal center, the second one being tentatively assigned to the formation of electrogenerated soluble short oligomers. In any case no formation of polymeric deposit occurs.

Appendix A. Supplementary material

CCDC 1531968-1531970 contain the supplementary crystallographic data for the complex **2a-c**. These data can be obtained free of charge via www.ccdc.cam.ac.uk/data_request/cif, by e-mailing (data_request@ccdc.cam.ac.uk), or by contacting The Cambridge Crystallographic Data Centre 12 Union Road Cambridge CB2 1EZ, UK. Fax: þ44(0)1223-336033.

Appendix B. Supplementary material

Intermolecular hydrogen bond interactions in the solid state structures of **2a-c** (Fig. S1), selected bond distances and angles for **2a** and **2c** (Table S1), hydrogen bonds in **2a-c** (Table S2), and cartesian coordinates and total energy of the DFT-computed complexes (Table S3).

Supplementary data associated with this article can be found, in the online version, at http://dx.doi.org/10.1016/j.ica

Acknowledgments

References

[1] E.V. Shchegolkov, Y.V. Burgart, O.G. Khudina, V.I. Saloutin, O.N. Chupakhin, Russ. Chem. Rev. 79 (2010) 31.

[2] (a) A.V. Kel'in, Curr. Org. Chem. 7 (2003) 1691; (b) A.V. Kel'in, A. Maioli, Curr. Org. Chem. 7 (2003) 1855.

[3] R.M. Pike, Coord. Chem. Rev. 2 (1967) 163.

[4] A.D. Garnovskii, B.I. Kharisov, L.M. Blanco, D.A. Garnovskii, A.S. Burlov, I.S. Vasilchenko, G.I. Bondarenko, J. Coord. Chem. 46 (1999) 365.

[5] D.J. Otway, W.S. Rees, Coord. Chem. Rev. 210 (2000) 279.

[6] A.E.V. Gorden, J. Xu, K.N. Raymond, Chem. Rev. 103 (2003) 4207.

[7] J.F. Da Silva, W. Martins, Talanta 39 (1992) 1307.

[8] O. Hiroyuki, H. Naoki, M. Kotaro, S. Kojiro, N. Hirochika, I. Hisanori, J. Soc. Anal. Chem. 26 (2010) 607.

[9] J.A. Pretorius, J.C.A. Boeyens, J. Inorg. Nucl. Chem. 40 (1978) 1745.

[10] X. Cun-Jin, B.-G. Li, J.-T. Wan, B. Zhi-Yang, J. Lumin. 131 (2011) 1566.

[11] M.P. Rigobello, L. Messori, G. Marcon, M.A. Cinellu, M. Bragadin, A. Folda, G. Scutari, A. Bindoli, J. Inorg. Biochem. 98 (2004) 1634.

[12] J. Roncali, Chem. Rev. 92 (1992) 711.

[13] J. Roncali, J. Mater. Chem. 9 (1999) 1875.

[14] G.R. Whittell, I. Manners, Adv. Mater. 19 (2007) 3439.

[15] P. Audebert, P. Capdevielle, M. Maumy, New J. Chem. 16 (1992) 697.

[16] R.P. Kingsborough, T.M. Swager, J. Am. Chem. Soc. 121 (1999) 8825.

[17] M.O. Wolf, Adv. Mater. 13 (2001) 545.

[18] R.P. Kingsborough, T.M. Swager, Chem. Mater. 12 (2000) 872.

[19] B. Song, S. Yang, H. Zhong, L. Jin, D. Hu, G. Liu, J. Fluor. Chem. 126 (2005) 87.

[20] G. Magueur, B. Crousse, S. Charneau, P. Grellier, J.-P. Bégué, D. Bonnet-Delpon, J. Med. Chem. 47 (2004) 2694.

[21] S.A. Gamage, J.A. Spicer, G.W. Rewcastle, J. Milton, S. Sohal, W. Dangerfield, P. Mistry, N. Vicker, P.A. Charlton, W.A. Denny, J. Med. Chem. 45 (2002) 740.

[22] I.M. Abdou, A.M. Saleh, H.F. Zohdi, Molecules 9 (2004) 109.

[23] G. Malandrino, L.M.S. Perdicaro, G. Condorelli, I.L. Fragalà, P. Rossi, P. Dapporto, Dalton Trans. (2006) 1101.

[24] G. Ahumada, T. Roisnel, S. Sinbandhit, C. Manzur, D. Carrillo, J.-R. Hamon, J. Organomet. Chem. 737 (2013) 1.

[25] S. Celedon, M. Fuentealba, T. Roisnel, J.-R. Hamon, D. Carrillo, C. Manzur, Inorg. Chim. Acta 390 (2012) 184.

[26] G. Ahumada, T. Roisnel, J.-R. Hamon, D. Carrillo, C. Manzur, J. Chil. Chem. Soc. 58 (2013) 1842.

[27] A. Trujillo, M. Fuentealba, D. Carrillo, C. Manzur, I. Ledoux-Rak, J.-R. Hamon, J.-Y. Saillard, Inorg. Chem. 49 (2010) 2750.

[28] S. Celedón, V. Dorcet, T. Roisnel, A. Singh, I. Ledoux-Rak, J.-R. Hamon, D. Carrillo, C. Manzur, Eur. J. Inorg. Chem. (2014) 4984.

[29] J.-P. Costes, Polyhedron 6 (1987) 2169.

[30] G. Ahumada, D. Carrillo, C. Manzur, M. Fuentealba, T. Roisnel, J.-R. Hamon, J. Mol. Struct. 1125 (2016,) 781.

[31] (a) M. Fuentealba, J.-R. Hamon, D. Carrillo, C. Manzur, New J. Chem. 31 (2007) 1815; (b) A. Trujillo, S. Sinbandhit, L. Toupet, D. Carrillo, C. Manzur, J.-R. Hamon, J. Inorg. Organomet. Polym. Mater. 18 (2008) 81.

[32] M. Fuentealba, A. Trujillo, J.-R. Hamon, D. Carrillo, C. Manzur, J. Mol. Struct. 881 (2008) 76.

[33] R.D. Archer, Inorg. Chem. 2 (1963) 292.

[34] N.G. Conelly, W.E. Geiger, Chem. Rev. 96 (1996) 877.

[35] A. Altomare, M.C. Burla, M. Camalli, G. Cascarano, C. Giacovazzo, A. Guagliardi, A.G.G. Moliterni, G. Polidori, R. Spagna, J. Appl. Crystallogr. 32 (1999) 115.

[36] G.M. Sheldrick, Acta Cryst. A64 (2008) 112.

[37] O.V. Dolomanov, L.J. Bourhis, R.J. Gildea, J.A.K. Howard, H. Puschmann, J. Appl. Crystallogr. 42 (2009) 339.

[38] (a) G. te Velde, F.M. Bickelhaupt, S.J.A. van Gisbergen, C. Fonseca Guerra, E.J. Baerends, J.G. Snijders, T. Ziegler, J. Comput. Chem. 22 (2001) 931. (b) ADF2013, SCM, Theoretical Chemistry, Vrije Universiteit, Amsterdam, The Netherlands, http://www.scm.com.

[39] J.P. Perdew, K. Burke, Y. Wang, Phys. Rev. B 54 (1996) 16533.

[40] E. Van Lenthe, E.J. Baerends, J. Comput. Chem. 24 (2003) 1142.

[41] K. Burke, E.K.U. Gross, (Lecture notes in physics). In: Joubert D, editor. A guided tour of time-dependent density functional theory, in density functionals: theory and applications, vol. 500, Springer, 1998.

[42] (a) J.A. Pretorius, C.A. Boeyens, J. Inorg. Nucl. Chem. 40 (1978) 1519; (b) M. Al-Anber, P. Ecorchard, T. Rüffer, H. Lang, Main Group Chem. 11 (2012) 205.

[43] J.A.O. Woods, H. Oluwatola Omoregie, N. Retta, F. Capitelli, I. Da Silva, Synth. React. Inorg. Met. Org. Nano-Met. Chem. 39 (2009) 704.

[44] D.F. Xu, Z.H. Shen, Y. Shi, Q. He, Q.C. Xia, Russ. J. Coord. Chem. 36 (2010) 458.

[45] K. Nakamoto, The Infrared Spectra of Inorganic and Coordination Compounds 3rd Edit.; Wiley-Interscience: New York, (1978).

[46] (a) P. Molina, A. Arques, I. Cartagena, Comprehensive Heterocyclic Chemistry III, Elsevier, New York, 2008, Vol. 3, Chapter 09, pp. 625-739; (b) J.J. Peron, P. Saumagne, J.M. Lebas, Spectrochim. Acta 1970, 26A, 1651.

[47] H.A. Jahn, E. Teller, Proc. R. Soc. London, Ser. A 161 (1937) 220.

[48] (a) I.B. Bersuker, Coord ; Chem. Rev. 14 (1975) 357; (b) R. Engelman, The Jahn-Teller Effect in the Molecules and Crystals, Wiley-Interscience, London, 1972.

[49] (a) A. Kuhn, S. Tischlik, K. H. Hopmann, M. Landman, P. H. van Rooyen, J. Conradie, Inorg. Chim. Acta 453 (2016) 345; (b) S. Layek, S. Kumari Anuradha, B. Agrahari, R. Ganguly, D. D. Pathak, Inorg. Chim. Acta 453 (2016) 735; (c) L.A.M. Baxter, A.J. Blake, R.O. Gould, G.A. Heath, T.A. Stephenson, Acta Crystallogr. Sect. C, 49 (1993) 1311.

[50] (a) R.-G. Xiong, X.-Z. You, J.-X. Dong, X.-Y. Huang, Acta Crystallogr. Sect ; C 51 (1995) 835; (b) I. Moustakali-Mavridis, A. Terzis, E. Hadjoudis, Acta Crystallogr. Sect C 43 (1987) 1389.

[51] S. J. Howell, C. S. Day, R. E. Noftle, Inorg. Chim. Acta 358 (2005) 3711.

[52] (a) F.H. Allen, O. Kennard, D.G. Watson, L. Brammer, A.G. Orpen, R. Taylor, J. Chem. Soc., Perkin Trans. 2 (1987) S1; (b) F.H. Allen, Acta Crystallogr. Sect. B, 58 (2002) 380.

[53] M.A. Al-Anber, Am. J. Phys. Chem. 2 (2013) 1.

[54] A.P.B. Lever, "Inorganic Electronic Spectroscopy", Elsevier, Amsterdam, 1980.

[55] J. Oyarce, L. Hernández, G. Ahumada, J. P. Soto, M. A. del Valle, V. Dorcet, D. Carrillo, J.-R. Hamon, C. Manzur, Polyhedron 123 (2017) 277.
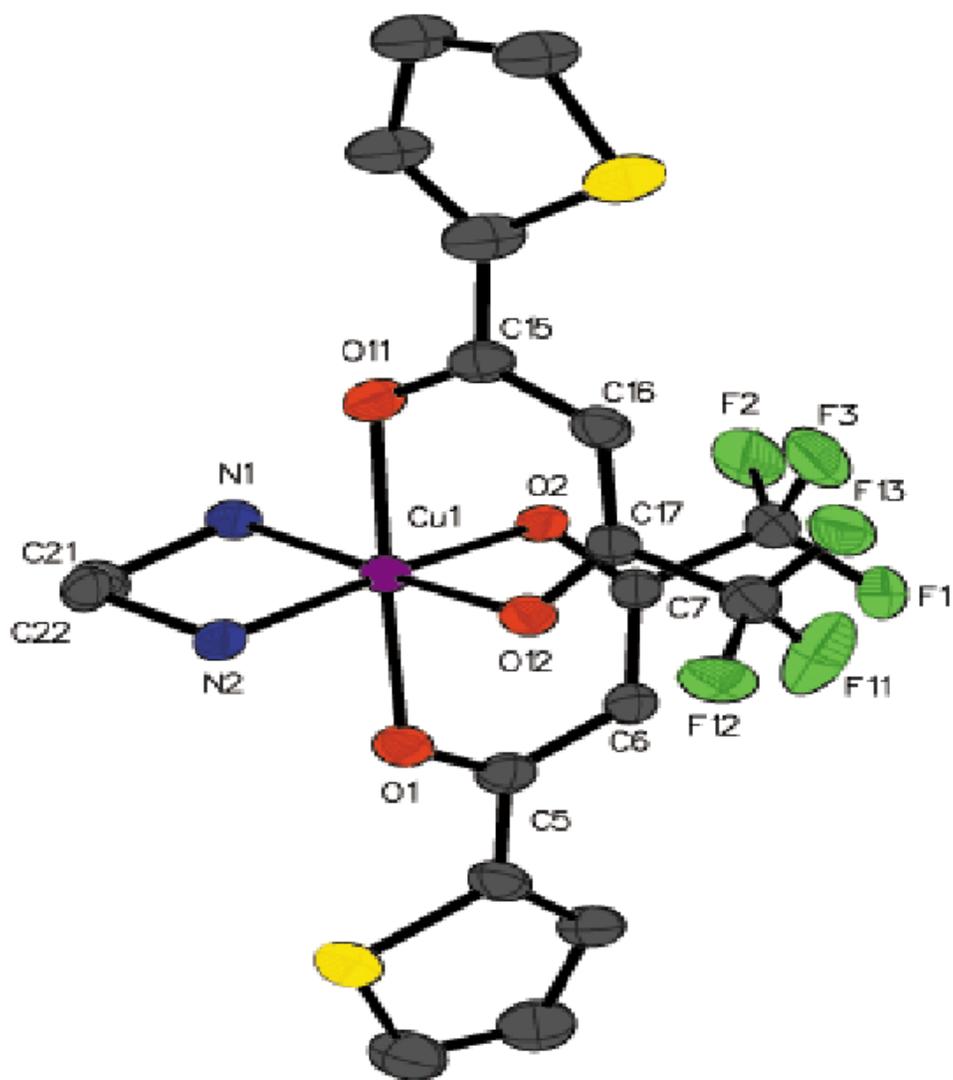
Graphical Abstract Synopsis

The three new six-coordinate bis(2-thenoyltrifluoroacetonato)-ethylenediamine Co(II), Ni(II) and Cu(II) complexes adopt a distorted octahedral geometry (pictured), with a significant elongation along the O-Cu-O axis due to Jahn-Teller effect. DFT and TDDFT calculations were performed to optimize geometries, describe electronic structures and interpret the major features of their UV-vis spectra.

HIGHLIGHTS

► Octahedral bis(2-thenoyltrifluoroacetonato)-ethylenediamine metal(II) complexes

► Characterization by elemental analysis, FTIR and ESI-MS techniques

► X-ray crystal structures of Co, Ni and Cu derivatives

► Geometry optimization and analysis of electronic structure using DFT calculations

► Interpretation of the major features of UV-vis spectra using TDDFT calculations